River Flow 2010 - Dittrich, Koll, Aberle & Geisenhainer (eds) - © 2010 Bundesanstalt für Wasserbau ISBN 978-3-939230-00-7

A method to estimate failure plane angle and tension crack depth

E. Amiri-Tokaldany
Department of Irrigation and Reclamation Engineering, Faculty of Agricultural Engineering and Technology, University of Tehran, Karaj, Iran

M. H. Dovoodi
The Research Centre of Soil Conservation, Tehran, Iran.

S. E. Darby
School of Geography, University of Southampton, Highfield, Southampton, SO17 1BJ UK

M. Taghavi
University of Tehran, Karaj, Iran

ABSTRACT: Among various types of riverbank failure, planar failure is the most common type, being associated with steep, relatively low banks composed of cohesive sediments. To analyse the stability of riverbanks against planar failure, many parameters including failure plane angle and the location and depth of tension crack have to be determined. In this research we have introduced a new analytical method to estimate the failure plane angle and also the amount of the bank retreat. Specifically, using field and laboratory data, a set of curves to estimate the tension crack depth is introduced. Using data from field study site, the results of the new method are compared with those obtained using existing models. The results show that the equations introduced in this research to estimate the failure plane angle, give a better agreement with the observations than the other models.

Keywords: Stability analysis, Tension crack depth, Riverbank, Planar failure, Factor of safety, Failure plane angle

1 INTRODUCTION

One of the sources of river sediment is riverbank failure among which planar failure is the most common type. This phenomenon usually happens in steep and relatively low height banks composed of cohesive sediments (Thorne, 1999). In such cases, riverbank stability analysis is typically undertaken by computing the ratio of resisting and driving forces applied to the most critical failure surface (Figure 1); i.e. $FS=FR_p/FD_p$, in which FS, FR_p, and FD_p = factor of safety with respect to bank failure, the resultant resisting force, and the resultant driving force, respectively.

There are a large number of riverbank stability analyses for planar failures (e.g. Osman and Thorne, 1988; Darby and Thorne, 1996; Rinaldi and Casagli, 1999; Simon et al., 2000; Amiri-Tokaldany et al., 2003, Samadi et al., 2009, among others), with each model varying in the ways they simulate the resisting and driving forces. According to Amiri-Tokaldany et al. (2003) the resultant driving and resisting forces acting on a unit width of the failure block can be written as follows:

$$FD_p = W \sin\beta - F_{cp} \sin\theta + H_{tw} \cos\beta \quad (1)$$

$$FR_p = CL + S \tan\phi^b + (W \cos\beta + F_{cp} \cos\theta - U - H_{tw} \sin\beta) \times \tan\phi \quad (2)$$

Where β = the failure plane angle, θ = the angle between the direction of the resultant of the hydrostatic confining pressure and a normal to the failure plane, W = the weight of a unit width of the failure block, F_{cp} = the hydrostatic confining pressure acting on a unit width of the failure block, H_{tw} = the hydrostatic force exerted by any water present in the tension crack on a unit width of the failure block, C = the effective cohesion of the bank material acting along the surface of failure plane, L = the length of the failure plane, S = the resultant negative pore water pressure, ϕ^b = the angle expressing the rate of strength increase relating to the negative pore water pressure, U = the resultant uplift force or positive pore water pressure acting on a unit width of the failure block, and ϕ = the effective internal friction angle of bank material (Figure 1).

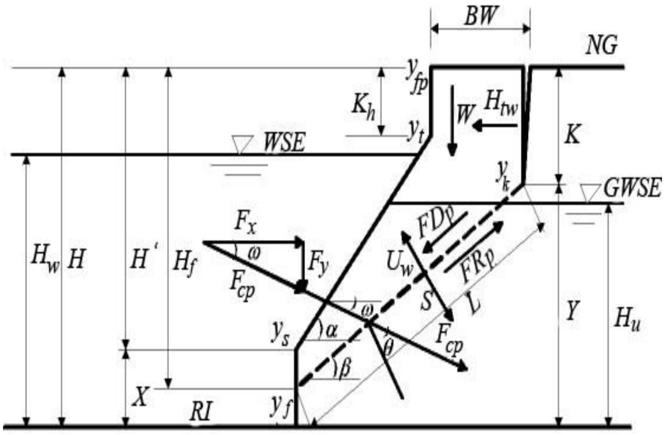

Figure 1 The framework for the riverbank stability analysis used herein, illustrating the forces exerted on an incipient failure block. H = height of riverbank; WSE = level of the water in river; RI = elevation of the river bed; BW = location of the tension crack or the magnitude of the bank retreat; NG = natural ground level; $GWSE$ = level of the ground water; α and β = angles of riverbank before and after bank failure, respectively; and K= depth of the tension crack. Points y_t, y_s, y_f, y_{fp} and y_k along with the heights H', X, and Y are used to define the geometry of the riverbank (After Samadi et al., 2009)

From Figure 1 and Equations (1) and (2) it is evident that the failure plane angle (β) and tension crack depth (K), define the failure block geometry, and thus play an important role on the stability analysis of the riverbank. Unfortunately, neither β nor K can be measured directly prior to bank failure, so it follows that accurate estimation of the factor of safety requires accurate prediction of these parameters. Many researchers have developed models to predict foresaid factors; e.g. Osman and Thorne (1988), Alonso and Combs (1990), Darby and Thorne (1996), Amiri-Tokaldany et al. (2003), among others. In terms of tension cracks, there are some published paper on determining the depth and location of tension cracks; e.g. Lohnes and Handy's (1968), Darby and Thorne (1994), Langendoen and Simon (2008), among others. However, the validity of them is undermined, while there is no analytical solution to determine the failure plane angle. In this research a method to determine the failure plane angle and tension crack depth is introduced.

2 MODEL DEVELOPMENT

2.1 *Failure Plane Angle*

As stated above, bank stability is modeled using a factor of safety as defined in Equations (1), and (2). To determine the failure plane angle, and the depth of the tension crack, it is first necessary to define all the known parameters in Equations (1) and (2) so that they can be solved to determine these two unknowns. Based on Figure 1, the weight of the failed block can be determined using:

$$W = \frac{A_W}{tan\,\beta} - B_W \tag{3}$$

in which A_w and B_w are defined in Table 1.

Table 1. Equations used to calculate A_w and B_w. See Figure 1 for definitions of symbols

Bank Geometry type	Bank Geometry Specification	A_w	B_w
I	$y_k = y_t = y_{fp}$ & $y_f = y_s$	$\gamma_s H^2/2$	$\gamma_s H^2/2tan\,\alpha$
II	$y_k = y_t = y_{fp}$ & $y_f < y_s$	$\gamma_s H^2/2$	$\gamma_s H'^2/2tan\,\alpha$
III	$y_k < y_t = y_{fp}$ & $y_f = y_s$	$\gamma_s(H^2-K^2)/2$	$\gamma_s H^2/2tan\,\alpha$
IV	$y_k < y_t = y_{fp}$ & $y_f < y_s$	$\gamma_s(H^2-K^2)/2$	$\gamma_s H'^2/2tan\,\alpha$
V	$y_k, y_t < y_{fp}$ & $y_f = y_s$	$\gamma_s(H^2-K^2)/2$	$\gamma_s(H^2-K_h^2)/2tan\,\alpha$
VI	$y_k, y_t < y_{fp}$ & $y_f < y_s$	$\gamma_s(H^2-K^2)/2$	$\gamma_s(H'^2-K_h^2)/2tan\,\alpha$

Moreover, the angle of θ (Figure 1) is defined as:

$$\theta = 90 - (\beta + \omega) \tag{4}$$

where ω = the angle between the resultant of hydrostatic pressure and the horizontal line (Figure 1). The hydrostatic pressure for different water levels within the river, and for different bank geometry configurations, can be determined using the equations listed in Table 2.

By rearrangement, the force resulting from the negative pore water pressure (S), is determined using:

$$S = \frac{A_S}{sin\,\beta} \tag{5}$$

where A_S depends on the bank geometry and the magnitude of the capillary height rise within the soil particles. If measurements of the soil matric tension are available, the following equation can be used to determine A_S directly:

$$A_S = \frac{\gamma_w}{2} h\, L \tag{6}$$

in which h = the matric suction and L = the effective length affected by matric suction. The hydrostatic force resulting from the presence of water inside the tension crack is also determined from the relations introduced in Table 3.

Moreover, by taking into consideration all possible bank geometries and relative locations of water levels in the river and the bank, and by rearranging, the positive pore water pressure (U) can be determined using:

$$U = \frac{U_w}{cos\ \beta} \tag{7}$$

$$U_w = \left(\frac{A_U}{tan\ \beta} - B_U \right) \tag{8}$$

where A_U and B_U are parameters introduced for purposes of clarity and which represent the bank geometry and the relative positions of the water surface and ground water table elevations, respectively (Table 4).

Table 2 - Equations to calculate F_{cp} and ω for different bank geometry and the location of river water level. See Figure 1 for definitions of symbols

Bank Geometry Type	The location of River Water Level (WSE)	F_{cp}	ω
All types	$WSE \le y_f$	0.0	-
I, II, V	$y_f < WSE \le y_t$	$(H_w^2 \sqrt{1+cot^2\alpha})\,\gamma_w/2$	$tan^{-1}(cot\ \alpha)$
II, IV,VI	$y_f < WSE \le y_s$	$H_w^2\,\gamma_w/2$	0.0
II, IV,VI	$y_s < WSE \le y_t$	$(\sqrt{H_w^4 + (H_w - (H-H'))^4 cot^2\alpha})\,\gamma_w/2$	$tan^{-1}\left((H_w - (H-H'))^2 cot\ \alpha / H_w^2\right)$
V	$y_t < WSE \le y_{fp}$	$(\sqrt{H_w^4 + [(H-K_h)(2H_w-(H-K_h))]^4 cot^2\alpha})\,\gamma_w/2$	$tan^{-1}\left([(H-K_h)(2H_w-(H-K)]cot\ \alpha / H_w^2\right)$
VI	$y_t < WSE \le y_{fp}$	$(\sqrt{H_w^4 + [(H'-K_h)(2H_w-(H'-K_h))]^4 cot^2\alpha})\,\gamma_w/2$	$tan^{-1}\left([(H'-K_h)(2H_w-(H'-K)]cot\ \alpha / H_w^2\right)$

Table 3- Equations to determine the value of A_S and H_{tw}. See Figure 1 for definitions of symbols

Bank Geometry Type	The Location of Ground Water Table	Capillary Height within Soil	A_S	H_{tw}
All Bank Geometry Types	$GWSE > y_k$	-	0.0	$(H_w - (H-K))^2\,\gamma_w/2$
	$GWSE < y_k$	$h + GWSE > y_k$	$(H - H_w - K)^2\,\gamma_w/2$	0.0
		$h + GWSE < y_k$	$h^2\,\gamma_w/2$	0.0

At the point of incipient failure (i.e. for the case when $FD_p = FR_p$), and substituting Equations (3) to (10) into Equations (1) and (2), it can be shown that:

$$\begin{aligned}&\left(\frac{A_W}{\tan\beta} - \frac{B_W}{\tan\alpha}\right)\sin\beta - F_{cp}\sin(90-(\beta+\omega))\\ &+H_{tw}\cos\beta = \frac{C(H-K)}{\sin\beta} + \frac{A_S\tan\phi^b}{\sin\beta} +\\ &\left[\begin{aligned}&\left(\frac{A_W}{\tan\beta} - \frac{B_W}{\tan\alpha}\right)\cos\beta + F_{cp}\cos(90-(\beta+\omega))\\ &-H_{tw}\sin\beta - \left(\frac{A_U}{\tan\beta} - \frac{B_U}{\tan\alpha}\right)\csc\beta\end{aligned}\right]\tan\phi\end{aligned} \tag{9}$$

After rearrangement, this gives:

$$\begin{aligned}&(A_W - F_{cp}(cos\ \omega + sin\ \omega tan\ \phi) + B_W\ tan\ \phi + H_{tw})\ cos\ \beta\\ &-(B_W - F_{cp}(sin\ \omega - cos\ \omega tan\ \phi) - H_{tw}\ tan\ \phi)\ sin\ \beta -\\ &(C(H-K) + A_S\ tan\ \phi^b - A_U\ tan\ \phi)\ csc\ \beta -\\ &(A_W\ tan\ \phi)\frac{cos\ \beta}{tan\ \beta} - (B_U\ tan\ \phi)\ sec\ \beta = 0.0\end{aligned} \tag{10}$$

By considering that:

$$A = A_W - F_{cp}(cos\ \omega + sin\ \omega tan\ \phi) + B_W\ tan\ \phi + H_{tw} \tag{11}$$

$$B = B_W - F_{cp}(sin\ \omega - cos\ \omega tan\ \phi) - H_{tw}\ tan\ \phi \tag{12}$$

$$D = C(H-K) + A_S\ tan\ \phi^b - A_U\ tan\ \phi \tag{13}$$

$$E = A_W\ tan\ \phi \tag{14}$$

Table 4- Equations for calculating A_U and B_U for different Bank Geometry Type and at different locations of river and ground water level. See Figure 1 for definitions of symbols

Bank Geometry Type	The Location of River (*WS*E) and Ground (*GWS*E) Water Levels	A_u	B_u
All Types	$GWSE \le y_f$	0.0	0.0
All Types	$y_f < WSE = GWSE \le y_k$	$H_u^2 \gamma_w / 2$	0.0
III, IV,V,VI	$y_k < WSE = GWSE \le y_{fp}$	$(Y^2 - 2Y H_u)\gamma_w / 2$	0.0
II,IV,VI	$y_s < WSE \le y_t$	$H_u^2 \gamma_w / 2$	0.0
I,III,V	$y_f < GWSE < WSE \le y_k \le y_t$	$H_u^2 \gamma_w / 2$	$(H_u^2 - H_w^2)\gamma_w / 2tan\,\alpha$
I,III,V	$y_f < GWSE < WSE \le y_k \le y_t$	$H_u^2 \gamma_w / 2$	$(H_W - H_u) H_u \gamma_w / 2tan\,\alpha$
II,IV,VI	$y_f \le WSE \le y_s < GWSE < y_k \le y_t$	$H_u^2 \gamma_w / 2$	$(H_u - X)^2 \gamma_w / 2tan\,\alpha$
II,IV,VI	$y_s \le WSE < GWSE < y_k \le y_t$	$H_u^2 \gamma_w / 2$	$(H_u - X)^2 - (H_w - X)^2 \gamma_w / 2tan\,\alpha$
II,IV,VI	$y_s \le GWSE < WSE < y_k \le y_t$	$H_u^2 \gamma_w / 2$	$(H_u - X)(H_w - H_u)\gamma_w / tan\,\alpha$
III,V	$y_s \le WSE < GWSE < y_k \le y_t$	$(Y^2 - 2Y H_u)\gamma_w / 2$	$(H_u^2 - H_w^2)\gamma_w / 2tan\,\alpha$
III,V	$y_s \le WSE < GWSE < y_k \le y_t$	$(Y^2 - 2Y H_u)\gamma_w / 2$	$(H_w - H_u) H_u \gamma_w / 2tan\,\alpha$
IV,VI	$y_f \le WSE \le y_s < y_k < GWSE \le y_t$	$(Y^2 - 2Y H_u)\gamma_w / 2$	$(H_u - X)^2 \gamma_w / 2tan\,\alpha$
IV,VI	$y_k < GWSE \le y_t$ & $y_s < GWSE \le y_t$	$(Y^2 - 2Y H_u)\gamma_w / 2$	$(H_u - X)^2 - (H_w - X)^2 \gamma_w / 2tan\,\alpha$
IV,VI	$y_k \le GWSE < WSE \le y_t$	$(Y^2 - 2Y H_u)\gamma_w / 2$	$(H_u - X)(H_w - H_u)\gamma_w / tan\,\alpha$
V	$y_k \le y_t < GWSE$ & $y_s < GWSE \le y_t$	$(Y^2 - 2Y H_u)\gamma_w / 2$	$(2H_u^2 - (H - K_h)^2 - H_w^2)\gamma_w / 2tan\,\alpha$
V	$y_k \le y_t < GWSE$ & $y_t < GWSE \le y_{fp}$	$(Y^2 - 2Y H_u)\gamma_w / 2$	$(H_u - K_h)(H_w - H_u)\gamma_w / tan\,\alpha$
V	$y_s \le WSE \le y_t < GWSE \le y_k$	$H_u^2 \gamma_w / 2$	$(2H_u^2 - (H - K_h)^2 - H_w^2)\gamma_w / 2tan\,\alpha$
V	$y_t < GWSE \le y_k$ & $y_t < GWSE \le y_{fp}$	$H_u^2 \gamma_w / 2$	$(H_u - K_h)(H_w - H_u)\gamma_w / tan\,\alpha$
VI	$y_f \le WSE \le y_s < y_k \le y_t < GWSE$	$(Y^2 - 2Y H_u)\gamma_w / 2$	$(2(H_u - X)(H' - K_h) - (H' - K_h)^2)\gamma_w / 2tan\,\alpha$
VI	$y_k \le y_t < GWSE$ & $y_s < GWSE \le y_t$	$(Y^2 - 2Y H_u)\gamma_w / 2$	$(2(H_u - X)(H' - K_h) - (H' - K_h)^2 - (H_w - X)^2)\gamma_w / 2tan\,\alpha$
VI	$y_k \le y_t < GWSE$ & $y_t < GWSE \le y_{fp}$	$(Y^2 - 2Y H_u)\gamma_w / 2$	$(H_u - H_w)(H' - K_h)\gamma_w / tan\,\alpha$
VI	$y_f \le WSE \le y_s < y_t < GWSE \le y_k$	$H_u^2 \gamma_w / 2$	$(2(H_u - X)(H' - K_h) - (H' - K_h)^2)\gamma_w / 2tan\,\alpha$
VI	$y_s < WSE \le y_t < GWSE \le y_k$	$H_u^2 \gamma_w / 2$	$(2(H_u - X)(H' - K_h) - (H' - K_h)^2 - (H_w - X)^2)\gamma_w / 2tan\,\alpha$
VI	$y_t < GWSE \le y_k$ & $y_t < WSE \le y_{fp}$	$H_u^2 \gamma_w / 2$	$(H_u - H_w)(H' - K_h)\gamma_w / tan\,\alpha$

$$F = B_u \tan\phi \tag{15}$$

it is then possible to derive:

$$A\cos\beta - B\sin\beta - D\frac{1}{\sin\beta} - E\frac{\cos\beta}{\tan\beta} - F\frac{1}{\cos\beta} = 0.0 \tag{16}$$

By multiplying both sides of Equation (16) by $\left(-\frac{\tan\beta}{\cos\beta}\right)$, in turn this gives:

$$F\tan^3\beta + (B + D)\tan^2\beta + (F - A)\tan\beta + (D + E) = 0.0 \tag{17}$$

For $F = 0$ (cases 1 to 4 in Table 3), the failure plane angle can then be determined using:

$$\tan\beta = \frac{A \pm \sqrt{\Delta}}{2(B + E)}$$
$$\Delta = A^2 - 4(B + E)(D + E) \tag{18}$$

Hence, for $\Delta = 0$, there is only one possible root and the solution for β is unique. For $\Delta \ne 0$ there are two possible solutions for β, of which either both can be negative, both can be positive, or, one can be positive and the other one can be negative. Clearly, solutions that provide values of $\beta<0$ are not physically meaningful, as is any solution for which $\beta > \alpha$. In the event that both solutions for β provide positive values, but both are smaller than the bank angle; i.e. $0 < \beta_1 < \beta_2 < \alpha$, it can be noted that the stability of riverbanks has an inverse relation with the riverbank angle; that is as the riverbank angle decreases the riverbank becomes more stable. Similar to left or right limits, in mathematics, we may consider that for β_1 the factor of safety tends to unity from its right hand side (values bigger than 1), whereas for β_2 the factor of safety tends to unity from its left hand side (values less than 1). Hence, the smaller value of β (i.e., β_1) is chosen in these cases.

Otherwise, for $F \ne 0$, by taking:

$$\left(\tan\beta = T - \frac{B + D}{3F}\right) \tag{19}$$

Equation (17) is reduced to:

$$T^3 + pT + q = 0 \tag{20}$$

in which:

$$p = \frac{F - A}{F} - \frac{1}{3}\left(\frac{B + D}{F}\right)^2 \tag{21}$$

$$q = 2\left(\frac{B + D}{3F}\right)^3 - \frac{(F - A)(B + E)}{3F^2} + \frac{D + E}{F} \tag{22}$$

Hence, T can be calculated using:

$$T = \sqrt[3]{-\frac{q}{2} + \sqrt{\left(\frac{q}{2}\right)^2 + \left(\frac{p}{2}\right)^2}} - \sqrt[3]{\frac{q}{2} + \sqrt{\left(\frac{q}{2}\right)^2 + \left(\frac{p}{2}\right)^2}} \tag{23}$$

from which the failure plane angle is given by:

$$\beta = tan^{-1}\left(T - \frac{B + D}{3F}\right) \tag{24}$$

2.2 *Tension Crack Depth*

The depth of the tension crack is the only unknown parameter in the above equations and must therefore be determined prior to calculating the failure plane angle. Based on laboratory experiments and field observations, the tension crack depth is a function of the specific weight of the soil materials, the bank angle, and soil resistance characteristics (internal friction angle and apparent cohesion, C_a):

$$F_1(\phi, C_a, \gamma_s, \alpha, K) = 0.0 \tag{25}$$

The apparent cohesion includes the effective cohesion as well as any additional strength due to matric suction and/or plant roots. Since the number of parameters affecting the tension crack depth is small, the Rayleigh method of dimensional analysis can be used. Hence, Equation (25) can be written as:

$$K = \frac{1}{N}\gamma_s^a C_a^b \tag{26}$$

In which N = a non-dimensional stability number here. By considering the dimensions of the parameters in Equation (26), it can be seen that:

$$L = (ML^{-2}T^{-2})^a (ML^{-1}T^{-2})^b \tag{27}$$

which implies that:

$$a + b = 0.0 \quad and \quad a + 2b = -1$$
$$\Rightarrow a = -1 \quad and \quad b = 1$$
$$K = \frac{1}{N}\gamma_s^{-1} C_a \Rightarrow N = \frac{C_a}{K\,\gamma_s} \tag{28}$$

Hence:

$$F_2(\alpha, \phi, N) = 0.0 \tag{29}$$

To define a form for this relation, it is necessary to employ empirical data defined using either laboratory or field experiments. Laboratory data are especially attractive for this purpose since the controlled conditions under which they are obtained are more amenable for precisely discriminating bank geometries immediately before and after the bank failure, the time of bank failure, as well as the precise mechanism of bank failure. In contrast, such information is not typically accessible within the field, where data are usually gathered some time after bank failure events. It is perhaps surprising, therefore, that physical models of riverbank failure have not previously been widely used in the literature and as a result there is a substantive lack of empirical information about the real situation of riverbanks at the time of failure. In this research, we therefore employ data from a novel set of laboratory experiments and event-based field data.

3 LABORATORY SIMULATED BANK FAILURE

To define the form of Equation (29) which indicates the relationship between tension crack depth and the controlling parameters, and to gather high-quality data for the purpose of model validation (see Section 4), we designed a novel physical model to conduct a series of experiments under highly controlled conditions. Since during the process of riverbank mass failure, the flow of water has no effective role upon this phenomenon, the flow pattern is omitted, but to enter the effects of hydrostatic water pressure against riverbank, the physical model is constructed using a range (see below) of sandy and sandy-silt materials inside a rectangular box with a length of 180 cm, height of 100 cm and width of 60 cm. We installed two control valves at different positions to apply different water depths against the bank constructed inside the box (Figure 2).

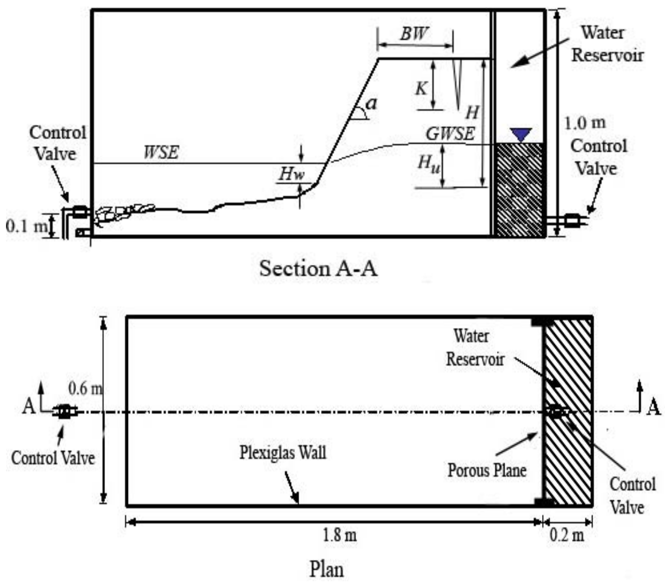

Figure 2 A schematic plan and cross section of the physical model used in the riverbank failure experiments. Note that in this case, H'=H=H_f

In Figure 2 H_w, H_u are the depth of water in the river and the depth of ground water above the bank toe, respectively. Experiments were conducted using 4 different types of uniform sediment, with mean grain sizes of 2.5, 1.5, 0.25, and 0.05 mm, respectively. For each material a total of 5 bank failures were induced by varying γ_s, ϕ, H, H', and α, giving a total of 20 experimental bank failures. For each material, specific weight was measured using sand core tests, while the soil cohesion and internal friction angle values were obtained via direct shear tests. To measure the value of the geometrical parameters of banks before and after bank failure, graduated measuring scales were attached to the box so that it was easy to precisely (to within ± 1 mm) read and record these parameters during each experiment.

To apply a hydrostatic confining force upon the bank, and to create the ground water table, both varying gradually over time, the opening of both valves was adjusted to create a range of hydrographs with arbitrary shapes. In addition to the data obtained from the laboratory experiments, we also employed a field data set which included measurements of tension crack depth from three streams (Long Creek, Goodwin Creek and Hotophia Creek) in northern Mississippi, USA (Thorne et al., 1981). These data lend confidence to the parameterization of the form of the tension crack depth relationship (Equation 30). For each of these groups of data, we calculated the dimensionless stability number (N), as defined in Equation (30), and by considering the magnitudes of the internal friction and bank angle, we developed the group of curves shown in Figure 3. In this way, for given values of internal friction angle and riverbank angle, the value of N may be estimated from Figure 3, from which the tension crack depth can then be estimated. During and after each laboratory experiment, the amount of β, K, and BW were measured carefully to be able to compare them with those obtained using the method described above; i.e. β which obtained using Equation (24) and K which obtained using Figure 3. Based on Figure 1, BW can be estimated when the amounts of β and K are known.

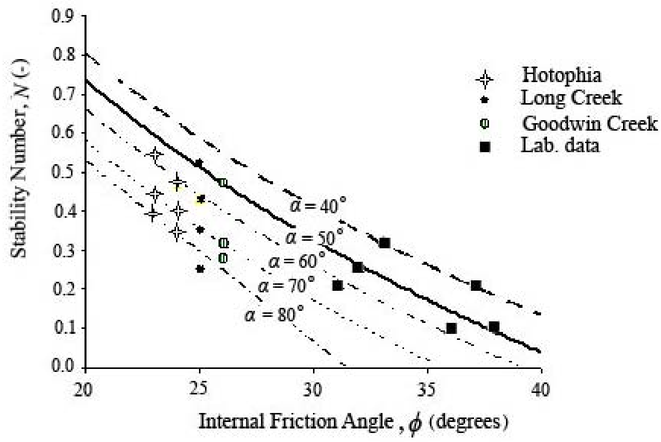

Figure 3 Relationship between the dimensionless stability number (N) and internal friction angle (ϕ) for a range of different riverbank angle as derived from laboratory experiments and field data

4 LIMITATIONS OF THE NEW MODEL

The new method presented here takes into account the effects of a wide range of parameters in riverbank stability. However, some limitations remain. The major limitation is that the model can only be applied for homogenous riverbanks. The effects of vegetation have not been considered and, in calculating the pore water pressure, it is assumed that the phreatic surface is parallel to the floodplain surface. The distribution of water pressure in the channel adjacent to the bank is also assumed to be hydrostatic.

5 ASSESSMENT OF MODEL PERFORMANCE

To evaluate the model performance and to summarize the accuracy of the present equations, first, we determined the mean relative error (MRE) of each prediction using:

$$MRE = \frac{1}{n}\sum_{i=1}^{n}\frac{\left|Observed_{(i)} - Predicted_{(i)}\right|}{Observed_{(i)}} \qquad (30)$$

where n = the number of tests, and $Observed_{(i)}$ and $Predicted_{(i)}$ = the observed and predicted values of the parameters of interest, respectively. The values of *MRE* for β, *K*, and *BW* so obtained are annotated on Table 4 and indicate that the new model predicts the failure plane angle very well (*MRE* = 4%) though the ability to predict the values of tension crack depth (*MRE* = 23%) and bank retreat (*MRE* = 27%) is not so good. The larger values of *MRE* for tension crack depth and bank retreat is, in part, related to the types of soil materials used for laboratory experiments. The materials of soil type 1 to 3 were non cohesion, whereas soil type number 4 includes some cohesive materials, are necessary to create tension cracks. So as shown in Table 4, *MRE* of tension crack depth and bank retreat for soil type number 4 is only 16.10 and 13.34%, respectively, which is considerably less than the amount of *MRE* for the soil number 1 and also the average amount of all tests. Hence, it seems that for cohesive soil materials, the present model should provide better results than non-cohesive materials.

To compare the accuracy of the new model, the *MRE* for β, *K*, and *BW* as derived for a range of different models is shown in Table 5. These data clearly reveal that the predictions obtained from the new equations developed herein represent an improvement over existing methods.

6 CONCLUSION

In this research we have introduced a new analytical method to estimate the failure plane angle. Using a combination of field and laboratory data, we provide a set of empirical curves that are used to estimate the tension crack depth. We found that the new model provides a mean relative error (*MRE*) of 4%, 23%, and 27% between calculated and observed values of failure plane angle, tension crack depth, and bank retreat, respectively. Hence, the approach presented here, can be used to determine the geometrical parameters of the failed blocks of riverbanks subject to planar failure.

ACKNOWLEDGMENTS

A part of this research was financially supported by the Office of Research Affairs of the University of Tehran under contract 1/7102017/03. Laboratory tests were carried out at the Research Institute for Water Scarcity and Drought. The authors would like to express their sincere thanks for this support.

Table 4- The Mean Relative Error of failure plane angle, tension crack depth and bank retreat for 4 types of materials used in laboratory experiments

Soil Type Number	Soil type description	β	*K*	*BW*
1	Cohesion-less	4.54(5)	55.62(4)	25.55(5)
2	Cohesion-less	4.24(3)	14.06(5)	44.37(5)
3	Cohesion-less	2.78(4)	11.24(5)	20.06(5)
4	Cohesive	5.13(2)	16/10(4)	13.34(4)
Average *MRE* (%)	-	4(14)	23(18)	26.5(19)

Note: The numbers inside parenthesis indicate the number of successful experiments for each soil type

Table 5- Comparing MRE of different methods for calculating β, *K*, and *BW*

Method	Overall Mean Relative Error, *MRE* (%)		
	β	*K*	*BW*
Lohnes and Handy (1966)	19	37.1	7.25
Osman and Thorne (1988)	34	37.3	6.75
Alonso and Combs (1990)	23	36.9	4.15
The new method	4	23	27

REFERENCES

Alonso, C. V., Combs, S. T., 1990. Streambank erosion due to bed degradation. A model concept, Trans. ASAE 33, 1239-1248.

ASCE Task Committee on Hydraulics, Bank Mechanics, and Modelling Adjustment, 1998. River Width Adjustment. I: Processes and mechanisms. Journal of Hydraulic Engineering, ASCE, 124: 881-902.

Amiri-Tokaldany, E., Darby, S.E., Tosswell, P., 2003. Bank stability analysis for predicting reach-scale land loss and sediment yield. Journal of the American Water Resources Association 39, 897-909.

Baker, R., 1981. Tensile strength, tension cracks, and stability of slopes, Soils and Foundations. Japanese Society of Soil Mechanics and foundation Engineering 21, 1-17.

Dapporto, S., Rinaldi, M., Casagli, N., Vannocci P., 2003. Mechanisms of riverbank failure along the Arno River, central Italy. Earth Surface Processes and Landforms 28, 1303-1323.

Darby, S. E., Thorne, C. R., 1994. Prediction of tension crack location and riverbank erosion hazards along destabilized channels. Earth Surface Processes and Landforms 19, 233-245.

Darby, S. E., Thorne, C. R., 1996. Development and testing of riverbank-stability analysis. Journal of Hydraulic Engineering, ASCE 122, 443-454.

Lohnes, R. A., and Handy, R. L., 1968. Slope angles in friable loess. The Journal of Geology 76, 247-258.
Langendoen, E. J. Simon, A., 2008. Modelling the Evolution of Incised Streams: II: Streambank erosion. Journal of Hydraulic Engineering, ASCE 134 (7), 905-915.
Osman, A. M., Thorne, C. R., 1988. Riverbank stability analysis. I: theory. Journal of Hydraulic Engineering, ASCE 114, 134 -150.
Rinaldi, M., Casagli, N., 1999. Stability of stream-banks formed in partially saturated soils and effects of negative pore water pressures: the Sieve River (Italy). Geomorphology 26, 253-277.
Samadi, A., Amiri-Tokaldany, E., Darby, S.E., 2009, Identifying the effects of parameter uncertainty on the reliability of riverbank stability modeling. Geomorphology,106,219-230.
Simon, A., Curini, A., Darby, S. E., Langendoen, E. J., 2000, Bank and near-bank processes in an incised channel. Geomorphology, 35, 193-217.
Spangler, M. G., Handy, R. L., 1982. Soil engineering. 4th Ed., In text Educational, New York, N. Y.
Taylor, D. W., 1948. Fundamental of soil mechanics. John Wiley & Sons, Inc., New York, N.Y.
Thorne, C. R., 1982. Processes and mechanisms of riverbank erosion. Gravel-bed rivers, R. D. Hey, J. C. Bathurst, and C. R. Thorne, eds., John Wiley & Sons, Inc., Chichester, U.K., 227-271.
Thorne, C.R., 1999. Bank processes and channel evolution in the incised rivers of North-Central Mississippi. In: Darby, S.E., Simon, A. (Eds.), Incised River Channels: Processes, Forms, Engineering and Management, John Wiley & Sons, Ltd., Chichester, U.K., pp. 97-121.
Thorne, C.R., Murphey, J.B., Little, W.C. 1981. Stream Channel Stability Appendix D: Bank stability and bank material properties in the bluffline streams of northwest Mississippi. Rep. Prepared For U. S. Army Corps of Engrs., Vicksburg District, Vicksburg, Miss, USDA Sedimentation Lab, Oxford, Mississippi.
Thorne, C. R., Abt, S. R., 1993. Analysis of riverbanks instability due to toe scour and lateral erosion. Earth Surface Processes and Landforms 18, 835-843.